AIAA JOURNAL
Vol. 35, No. 2, February 1997

High-Lift Aerodynamic Computations with One- and Two-Equation Turbulence Models

P. Godin* and D. W. Zingg†
University of Toronto, Downsview, Ontario M3H 5T6, Canada
and
T. E. Nelson‡
de Havilland Inc., Downsview, Ontario M3K 1Y5, Canada

The Spalart–Allmaras one-equation turbulence model and the Menter two-equation turbulence model are assessed for Navier–Stokes computations of high-lift aerodynamic flows, including cases with significant regions of separated flow. Cases considered include 1) separated flow over a single-element airfoil at high lift, 2) fully attached flows over the NLR 7301 airfoil and flap, and 3) separated flow over the GA(W)-1 airfoil and flap. For the single-element case, the Menter model provides better agreement with the experimental pressure distribution and velocity profiles. For the NLR 7301 airfoil and flap, both turbulence models provide excellent agreement with experimental pressures and skin-friction data. Velocity profiles are generally well predicted except in some parts of wakes. Turbulent shear stresses are not always well predicted. The predictions of the Spalart–Allmaras model are generally superior for this case, especially when boundary-layer confluence is important. For the GA(W)-1 airfoil and flap, the Menter model again provides better agreement in separated regions. Overall, the Spalart–Allmaras model is somewhat more robust and is thus preferred for general computations of aerodynamic flows, whereas the Menter model is preferred if separated flows are of primary interest.

Introduction

DURING the 1980s, turbulence modeling in Navier–Stokes computations of aerodynamic flows was generally accomplished using the Baldwin–Lomax algebraic model[1] and variations thereof. This model is adequate for many flows. However, difficulties can occur for transonic flows with strong shocks and separated flows. Improved results for shock strength and position can be obtained with the Johnson–King model.[2] In the 1990s, the Baldwin-Barth[3] and Spalart–Allmaras[4] one-equation turbulence models were introduced. These models provide several advantages over algebraic models, including improved accuracy in separated flows and wakes, while maintaining comparable robustness and efficiency. However, significant errors are still obtained in some separated flows. Furthermore, the effects of Reynolds number and flap gap are not always reliably predicted.[5] Consequently, there is still considerable interest in two-equation models, which have been successful in other flow problems. Although limited success was obtained using two-equation models for aerodynamic flows during the 1980s (Ref. 6), the zonal two-equation equation model of Menter,[7] which was introduced in 1993, shows considerable promise.

Evaluation of a new turbulence model proceeds in several phases. In the first phase, the model is applied to basic building-block flows. Because this is generally necessary for calibration, this phase must be performed by the model developers. In the second phase, the model is applied to a limited number of problems that are representative of the applications for which the model is intended. This phase is often carried out by the model developers as well. For example, Spalart and Allmaras[4] include results for airfoils at transonic speeds and airfoils with blunt bases in their original paper. Menter[7] shows results for an airfoil at high lift in his early work. In the third phase, the new model is applied to a broad range of cases using several different flow solvers. Several contributions have been made to the third phase of evaluation of the Baldwin–Barth, Spalart–Allmaras, and Menter turbulence models. Examples are given in Refs. 8–17.

This paper contributes to the continuing evaluation of the Spalart–Allmaras and Menter models with particular emphasis on multi-element airfoil geometries with separation. This is an important application for these models as algebraic models are inadequate for such flows. The purpose of this work is to provide an improved understanding of the range of applicability of the models. This will aid in selecting and applying the models as well as supplying useful feedback to the model developers.

The following flow cases are studied: 1) a single-element airfoil at low speed and high angle of attack with measurements by Doiron and Zingg,[18] 2) the National Aerospace Laboratory (NLR) 7301 airfoil and flap as tested by van den Berg[19] with two distinct gaps and two angles of attack, and 3) the GA(W)-1 airfoil with 29% chord Fowler flap, which was tested by Braden et al.[20] Quantities compared with experimental data include pressure coefficients, velocity profiles, and turbulent shear stress profiles.

Numerical Method and Turbulence Models

The flow solver used is a multiblock extension of the well-known code ARC2D.[21] It is an approximately-factored implicit algorithm that uses centered spatial differences with artificial dissipation to solve the compressible thin-layer Navier–Stokes equations. Standard values are used for all parameters, such as the artificial dissipation coefficients.[21] Further details are given in Ref. 9. The turbulence models are solved using a similar approach coupled with a subiteration scheme, as suggested by Spalart and Allmaras.[4]

Spalart–Allmaras Turbulence Model

The Spalart–Allmaras turbulence model[4] is a one-equation transport model written in terms of the eddy-viscosity-like term $\tilde{\nu}$. The equation is

$$\frac{D\tilde{\nu}}{Dt} = c_{b1}[1 - f_{t2}]\tilde{S}\tilde{\nu} + \frac{1}{\sigma}[\nabla \cdot ((\nu + \tilde{\nu})\nabla\tilde{\nu}] + \frac{c_{b2}}{\sigma}(\nabla\tilde{\nu})^2 - \left[c_{w1} f_w - \frac{c_{b1}}{\kappa^2} f_{t2}\right]\left(\frac{\tilde{\nu}}{d}\right)^2 + f_{t1}\Delta U^2$$

Presented as Paper 96-0567 at the 34th Aerospace Sciences Meeting, Reno, NV, Jan. 15–19, 1996; received March 5, 1996; revision received Oct. 4, 1996; accepted for publication Oct. 9, 1996; also published in *AIAA Journal on Disc*, Volume 2, Number 2.

*Graduate Student, Institute for Aerospace Studies, 4925 Dufferin Street.
†Associate Professor, Institute for Aerospace Studies, 4925 Dufferin Street. Member AIAA.
‡Senior Engineer, Aerodynamics Department, Garratt Boulevard. Member AIAA.

The kinematic eddy viscosity ν_t is related to the eddy viscosity term $\tilde{\nu}$ through the equation

$$\nu_t = \tilde{\nu} f_{v1}$$

where

$$f_{v1} = \frac{\chi^3}{\chi^3 + c_{v1}^3}$$

and

$$\chi = \tilde{\nu}/\nu$$

The production term $\tilde{S}$ in the differential equation is given by

$$\tilde{S} = S + (\tilde{\nu}/\kappa^2 d^2) f_{v2}$$

where S is the magnitude of the vorticity, d is the distance to the wall, and

$$f_{v2} = 1 - \frac{\chi}{1 + \chi f_{v1}}$$

The destruction function f_w is given by

$$f_w = g\left[\frac{1 + c_{w3}^3}{g^6 + c_{w3}^6}\right]^{\frac{1}{6}}$$

where

$$g = r + c_{w2}(r^6 - r)$$

and

$$r = \frac{\tilde{\nu}}{\tilde{S}\kappa^2 d^2}$$

The transition functions are

$$f_{t1} = c_{t1} g_t \exp\left[-c_{t2}(\omega_t^2/\Delta U^2)(d^2 + g_t^2 d_t^2)\right]$$

$$f_{t2} = c_{t3}\exp(-c_{t4}\chi^2)$$

where

$$g_t = \min\left(0.1, \frac{\Delta U}{\omega_t \Delta x_t}\right)$$

In the transition functions, d_t is the distance to the trip, ω_t is the vorticity at the trip, and Δx_t is the grid spacing at the trip. The velocity difference between a field point and the trip is ΔU. For multi-element airfoils there is a trip on the upper and lower surface of each element, and so a point in the field could refer to more than one trip. In this instance the closest trip of those on the correct surface of each airfoil is used. Because the effect of the trip is very localized, two trips are never close enough to cause a significant effect on the same field point. The constants used for the Spalart–Allmaras model are

$$c_{b1} = 0.1355 \qquad c_{b2} = 0.622$$

$$c_{t1} = 10.0 \qquad c_{t2} = 2.0 \qquad c_{t3} = 1.2 \qquad c_{t4} = 0.5$$

$$c_{w1} = c_{b1}/\kappa^2 + (1 + c_{b2})/\sigma \qquad c_{w2} = 0.3 \qquad c_{w3} = 2.0$$

$$c_{v1} = 7.1 \qquad \sigma = \tfrac{2}{3} \qquad \kappa = 0.41$$

As a result of difficulties with transition at low values of c_{t1}, we raised this constant to 10.0. According to Spalart and Allmaras,[4] c_{t1} has no effect on the solution other than as a transition trip, when it lies between 0.1 and 10.0.

Menter SST Turbulence Model

The Menter shear-stress transport (SST) turbulence model[7] is a two-equation transport model written in terms of the turbulent kinetic energy k and the specific turbulent dissipation rate ω. It combines the k-ω model with the k-ϵ model in a manner that exploits the best features of both. In addition, the model uses a modified constitutive relationship to account for the transport of the principal turbulent shear stress in adverse pressure gradients. The equations are

$$\frac{\mathrm{D}\rho k}{\mathrm{D}t} = \tau_{i,j}\frac{\partial u_i}{\partial x_j} - \beta^*\rho\omega k + \frac{\partial}{\partial x_j}\left[(\mu + \sigma_k\mu_t)\frac{\partial k}{\partial x_j}\right]$$

$$\frac{\mathrm{D}\rho\omega}{\mathrm{D}t} = \frac{\gamma}{\nu_t}\tau_{i,j}\frac{\partial u_i}{\partial x_j} - \beta\rho\omega^2 + \frac{\partial}{\partial x_j}\left[(\mu + \sigma_\omega\mu_t)\frac{\partial \omega}{\partial x_j}\right] + 2\rho(1 - F_1)\sigma_{\omega 2}\frac{1}{\omega}\frac{\partial k}{\partial x_j}\frac{\partial \omega}{\partial x_j}$$

The constant F_1 is a blending function that goes from one near the surface to zero away from the surface. The function F_1 is also used to blend the constants of the standard Wilcox k-ω model with those of the transformed k-ϵ model

$$\Phi = F_1\Phi_1 + (1 - F_1)\Phi_2$$

where Φ stands for any constant in the two differential equations.

The coefficients for the SST model are

$$\beta_1^* = 0.09 \qquad \sigma_{k1} = 0.85 \qquad \kappa = 0.41 \qquad a_1 = 0.31$$

$$\gamma_1 = \beta_1/\beta_1^* - \sigma_{\omega 1}\kappa^2/\sqrt{\beta^*} \qquad \beta_1 = 0.0750 \qquad \sigma_{\omega 1} = 0.5$$

$$\beta_2^* = 0.09 \qquad \sigma_{k2} = 1.0 \qquad \gamma_2 = \beta_2/\beta_2^* - \sigma_{\omega 2}\kappa^2/\sqrt{\beta^*}$$

$$\beta_2 = 0.0828 \qquad \sigma_{\omega 2} = 0.856$$

The blending function F_1 is given by

$$F_1 = \tanh(\Gamma_a^4)$$

where

$$\Gamma_a = \min[\max(\Gamma_1, \Gamma_3), \Gamma_2]$$

$$\Gamma_1 = \frac{500\nu}{y^2\omega} \qquad \Gamma_2 = \frac{4\rho\sigma_{\omega 2}k}{y^2 C D_{k-\omega}} \qquad \Gamma_3 = \frac{\sqrt{k}}{\beta^* \omega y}$$

$$C D_{k-\omega} = \max\left(\rho\frac{2\sigma_{\omega 2}}{\omega}\frac{\partial k}{\partial x_j}\frac{\partial \omega}{\partial x_j}; 10^{-20}\right)$$

After imposing the SST model constraint, the kinematic eddy viscosity ν_t is related to k and ω though the equation

$$\nu_t = \min\left[\frac{k}{\omega}, \frac{a_1 k}{\Omega F_2}\right]$$

The function F_2 is a blending function that is equal to one inside boundary layers and goes to zero for free shear layers:

$$\Gamma_b = \max(2\Gamma_3, \Gamma_1) \qquad F_2 = \tanh(\Gamma_b^2)$$

For general flows, Ω is the absolute value of vorticity. The boundary conditions for solid walls are

$$k_0 = 0 \qquad \omega_0 = 10\frac{6\nu}{\beta_1^*(\Delta y_1)^2} \quad \text{at} \quad y = 0$$

with Δy_1 being the distance between the wall and the first grid point away from the wall.

Results and Discussion

Single-Element Airfoil with Separation

The experimental data for this case are for a 17% chord thick airfoil with moderate aft loading at an angle of attack of 9.2 deg, a Reynolds number of roughly 1.7×10^6, and a Mach number of 0.15. The fine grid for the computations is a 347×297 C-grid generated with a hyperbolic grid generator. It has 229 points on the body (streamwise) and 60 points in the wake. Points are clustered at the leading edge, the trailing edge, and at 0.7 chord on the upper surface of the airfoil, near the separation point, where the streamwise spacing is 0.1% chord. Normal spacing at the body is 1×10^{-7} chord. The outer boundary is at 25 chords. A coarser grid, which is 175×149, is used to examine numerical errors. It was generated by removing every second grid point in each coordinate direction from

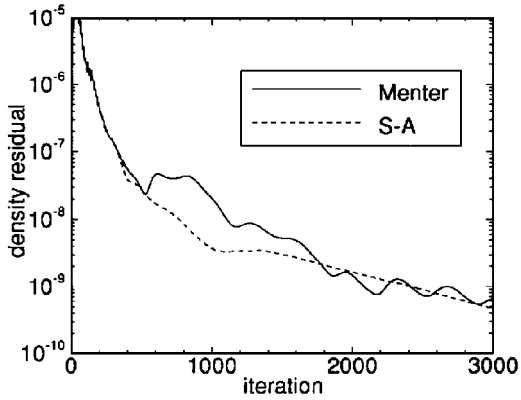

Fig. 1 Comparison of convergence histories for the single-element case.

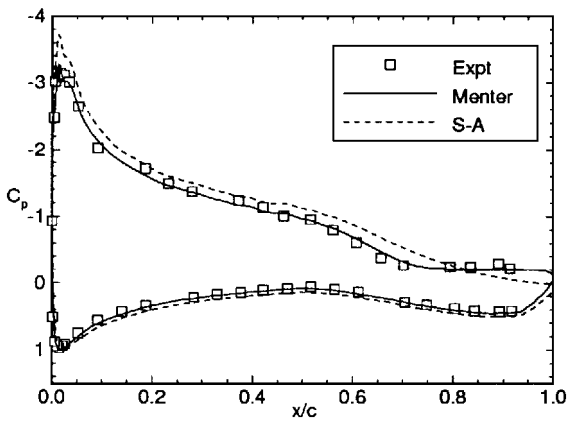

Fig. 2 Comparison of computed and experimental surface pressures for the single-element airfoil at $\alpha = 9.2$ deg.

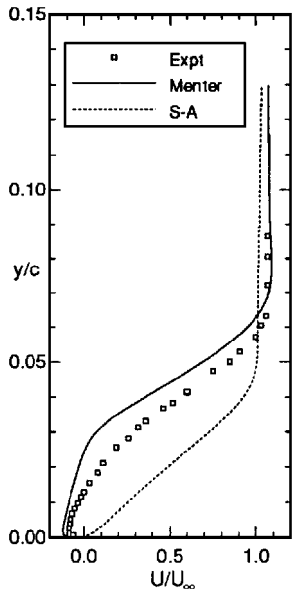

Fig. 3 Comparison of computed and experimental boundary-layer velocity profiles on the upper surface at $x/c = 0.95$.

the finer grid. Transition is fixed at 1.3% chord on the upper surface and 8% chord on the lower surface. Figure 1 shows the convergence histories for the Spalart–Allmaras and Menter models. Although the one-equation model converges slightly faster, the difference is small.

Computed and experimental surface pressures for the fine grid are compared in Fig. 2. The separation point is predicted reasonably well by both models. However, the Menter model correctly predicts the flattening of the pressure distribution near the trailing edge, and overall it predicts surface pressures within experimental tolerances. The lift is clearly overpredicted using the Spalart–Allmaras model.

In Fig. 3, the computed velocity profiles are compared with experimental data at station $x/c = 0.95$ on the upper surface. The Spalart–

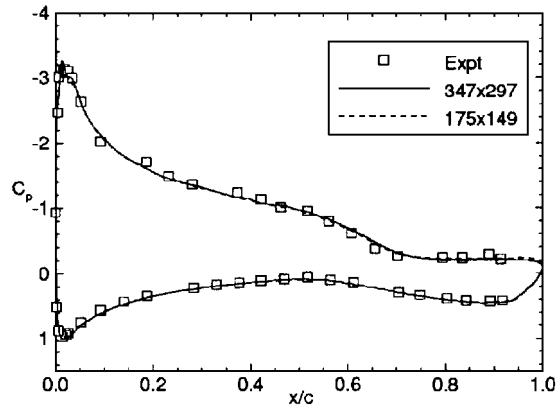

Fig. 4 Grid resolution study for the single-element case: pressure coefficient for the Menter model.

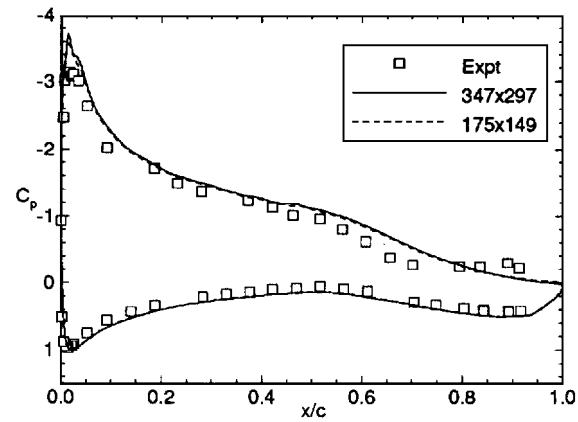

Fig. 5 Grid resolution study for the single-element case: pressure coefficient for the Spalart–Allmaras model.

Allmaras model predicts a separation bubble that is much too thin, whereas the Menter model predicts one that is too thick. The Menter model also predicts the velocity of the reversed flow fairly well.

Figures 4 and 5 compare the pressure distributions for the fine grid with those from the coarse grid. These figures show that numerical errors in the surface pressures are small. Slight differences occur only near the trailing edge of the airfoil for the Menter model, as shown in Fig. 4. For the Spalart–Allmaras model, slight differences occur across the upper surface, as shown in Fig. 5.

Grid resolution has a greater effect on the velocity profiles, as is shown in Fig. 6. However, the effect of grid resolution is much smaller than the effect of the turbulence model. This allows us to reliably compare the models.

NLR 7301 Airfoil and Flap

Case A: $\alpha = 13.1$ deg, Gap = 2.6% Chord

The NLR 7301 airfoil and flap configuration, as shown in Fig. 7, has a 32% chord flap and the flap angle is 20 deg. The overlap is 5.3% chord and the nominal gap setting is 2.6% chord. Tests were performed in the NLR wind tunnel at a Reynolds number of 2.51×10^6 and a Mach number of 0.185 with free transition. Two-dimensional flow was maintained by applying an appropriate amount of side wall blowing. This configuration is similar to a takeoff flap setting. Up to $\alpha = 13.1$ deg, which produces close to maximum lift, the flow is fully attached. Consequently, this is an excellent case to compare the boundary-layer velocity and turbulent stress profiles computed using various turbulence models.

A small deflection of the flap was noted in the experiment, and the deflected position was measured. The measured gap was 2.4% chord, and the estimated flap angle was 19.75 deg. The overlap was not affected. The measured flap position has been used here for the computations.

The grid used for the computations has a total of 182,295 nodes, and the off-wall spacing is 1×10^{-7} chord. Based on experimental observations, transition was fixed at 2.83% chord on the upper

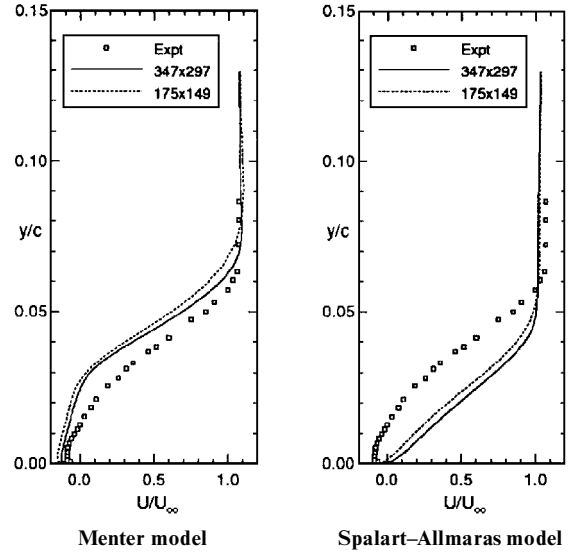

Fig. 6 Grid resolution study for the single-element case: velocity profiles.

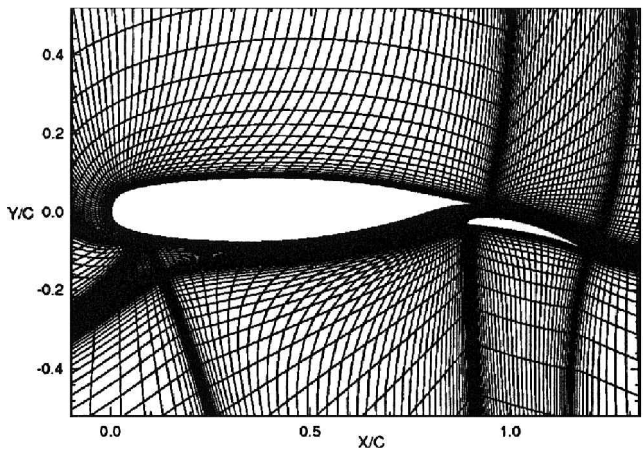

Fig. 7 Near-field grid, with every second grid line plotted, for the NLR 7301 airfoil and flap with gap = 2.6% chord.

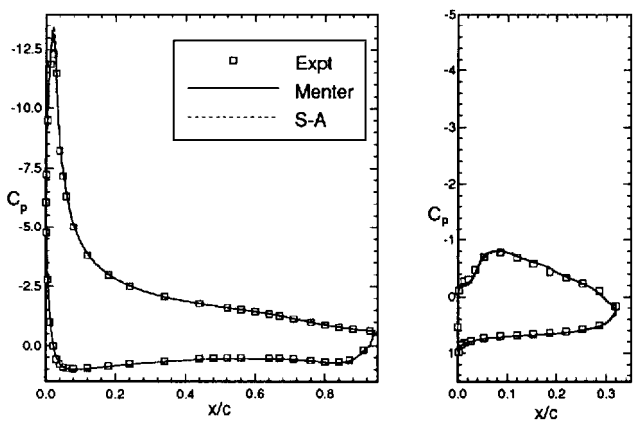

Fig. 8 Pressure distributions for the NLR 7301 airfoil with 20-deg flap and α = 13.1 deg.

surface of the main airfoil and at 72% chord on the lower surface. On the flap, transition was fixed at 17 and 31% chord on the upper and lower surfaces, respectively. On the upper surface of the main airfoil, the transition point is just downstream of the laminar separation point, leading to a separation bubble similar to that seen in the experiments. Streamwise grid resolution is increased in this region.

Convergence histories are not shown for this case since the solution was obtained by restarting from a lower angle of attack. A convergence history for $\alpha = 6$ deg is shown in the next section.

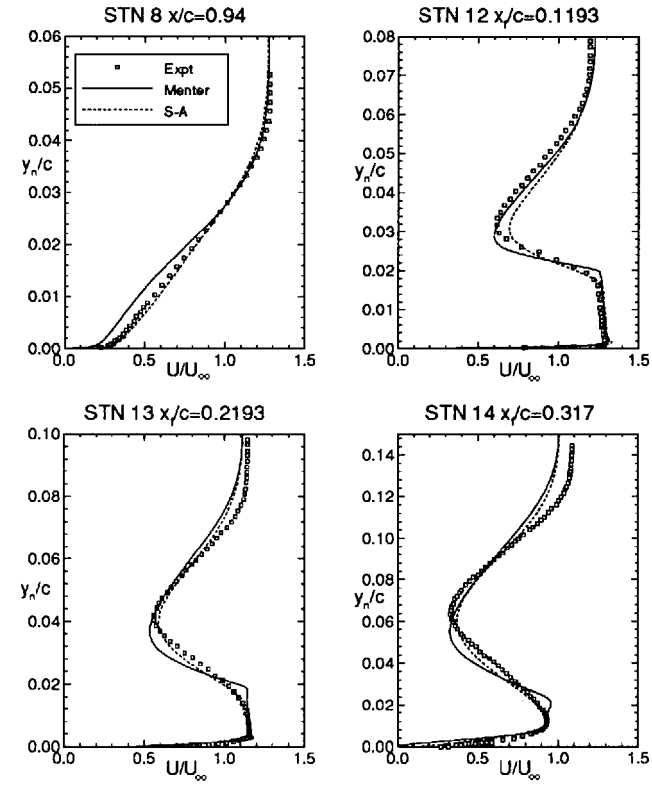

Fig. 9 Boundary-layer and wake velocity profiles for the NLR 7301 airfoil with 20-deg flap and α = 13.1 deg.

Figure 8 shows the computed surface pressure distributions. As expected, both models are very accurate.

Boundary-layer and wake velocity profiles are also well predicted, as shown in Fig. 9. Station 8 is on the upper surface of the main airfoil at the trailing edge. Stations 12, 13, and 14 are progressively farther downstream on the flap. Station 12 is downstream of the trailing edge of the main airfoil, and station 14 is at the flap trailing edge. Generally, the predictions of the Spalart–Allmaras model are superior for this case.

Figure 10 shows the turbulent shear stress profiles at the same four stations. The differences between the turbulence models are more apparent when looking at the turbulent shear stress. Figure 10 clearly shows the Spalart–Allmaras model outperforming the Menter model in predicting the flow subtleties.

Skin-friction coefficients on the upper surface of the main airfoil are compared with experiment in Fig. 11. Both turbulence models produce excellent agreement. With a grid spacing normal to the surface of 1×10^{-7} chord, the numerical errors in skin friction are very small.

The computations were repeated using a grid with 90,000 nodes. Changes in both surface pressures and velocity profiles are small. A grid resolution study for this case is described in Ref. 16.

Case B: α= 6.0 deg, Gap = 2.6 and 1.3% Chord

The next case considered is designed to assess the effectiveness of the turbulence models in simulating the effect of gap variation in a multi-element configuration. Predicting the change in lift resulting from a change in the gap is a difficult challenge for the turbulence models, as the confluence of the wake of the main airfoil and the boundary layer on the upper surface of the flap becomes important as the gap setting is reduced.

As for the α= 13.1 deg case, corrections to gap and flap angle were used for the gap = 2.6% chord. For the gap = 1.3% chord, no corrections were measured in the experiment, and so none were applied. Arguably, a similar correction is needed because the change is due to structural deformation of the flap brackets caused by airload on the flap.

Figure 12 shows the convergence histories obtained for the gap = 2.6% chord case at α = 6.0 deg. The Spalart–Allmaras model converges faster and further than the Menter model. Although this

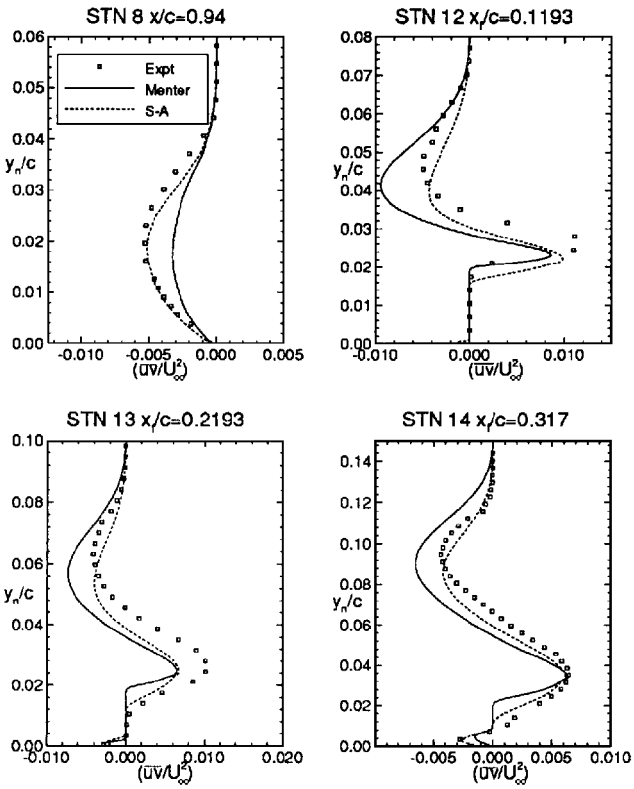

Fig. 10 Turbulent shear stress profiles for the NLR 7301 airfoil with 20-deg flap and $\alpha = 13.1$ deg.

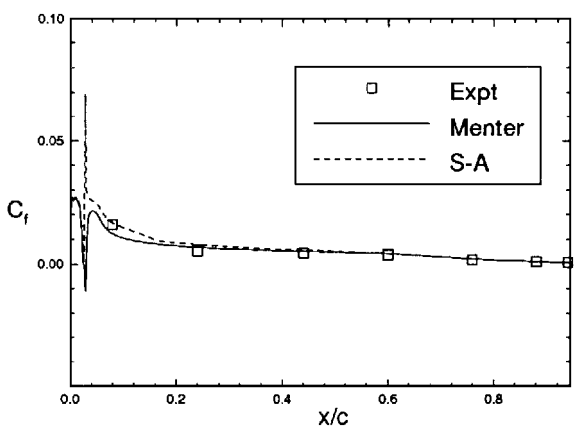

Fig. 11 Skin friction for the NLR 7301 airfoil with 20-deg flap and $\alpha = 13.1$ deg.

is not always the case, as shown in Fig. 1, the Spalart–Allmaras model is somewhat more robust than the Menter model. We have not found the Menter model to require finer grids near the surface, as some other researchers have found.[5] However, we already use a very small wall spacing to accurately determine skin friction.

Pressure distributions for the two gap settings are shown in Fig. 13. Experimentally, the difference in the lift coefficient between the two gap settings is 0.050. Using the Spalart–Allmaras model, a difference of 0.027 is obtained, whereas the Menter model leads to a difference of 0.005.

Velocity profile plots in Figs. 14 and 15 show that the Spalart–Allmaras model is superior in handling the merging of boundary layers and wakes. Experimental turbulent shear stress data for gap = 2.6% chord are shown in Fig. 16. Shear stress data are not available for the small gap case. Again, the Spalart–Allmaras predictions are closer to the experimental data.

GA(W)-1 Airfoil and Flap

Test case B1 from the experiment by Braden et al.[20] is typical of a landing flap configuration, as shown in Fig. 17, and represents

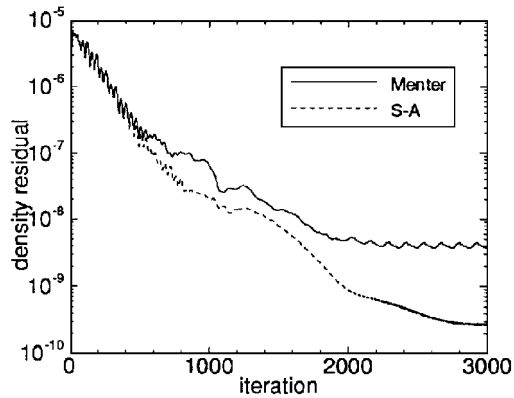

Fig. 12 Convergence histories for the NLR 7301 airfoil with 20-deg flap and $\alpha = 6.0$ deg.

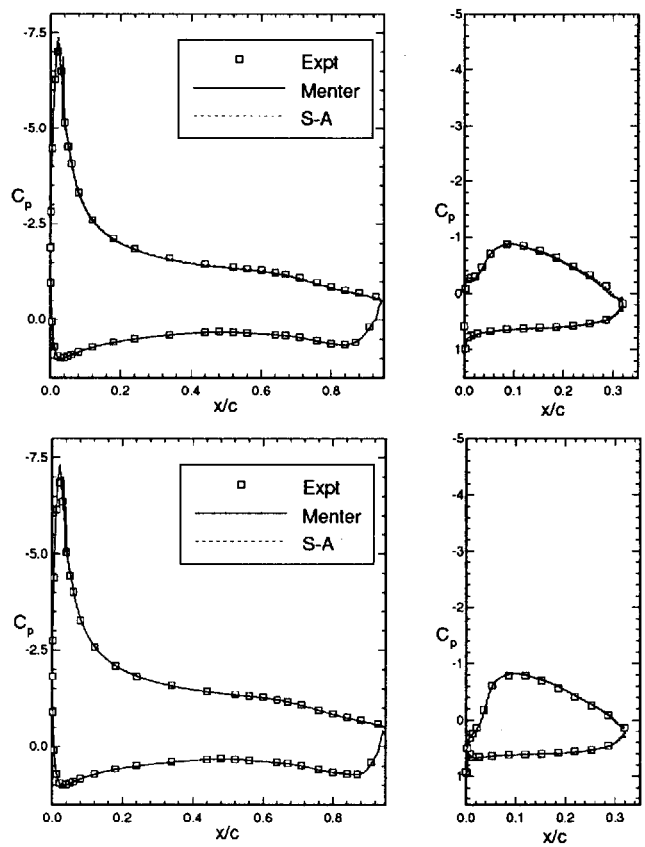

Fig. 13 Pressure distributions for the NLR 7301 airfoil with 20-deg flap and $\alpha = 6.0$ deg at two different gap settings. The upper plot is for a gap of 2.6% chord, and the lower is for a gap of 1.3% chord.

a difficult challenge for computational fluid dynamics codes. The flap angle is 30 deg with a gap of 4% chord and an overlap of 0.0% chord. The angle of attack for the case is 4.0 deg, $M = 0.116$, and $Re = 0.62 \times 10^6$. For these conditions, there is a large region of separated flow on the upper surface of the flap.

The grid used contains a total of 106,000 points in an H-type arrangement of 13 blocks. The off-wall spacing is 1×10^{-7} chord, and points are clustered near the leading and trailing edges and at the entrance to the cove on the main airfoil. The trailing edges of both elements were closed by symmetrically thinning the airfoil near the trailing edge.

The computed pressure distribution agrees quite well with the experimental data, as shown in Fig. 18. The Menter model is better in the separated region on the flap, but this does not appear to affect the loading on the main airfoil. This result for the Spalart–Allmaras model is better than that reported in Ref. 16. The primary difference is that the present grid has an increased streamwise density on the upper surface of the flap.

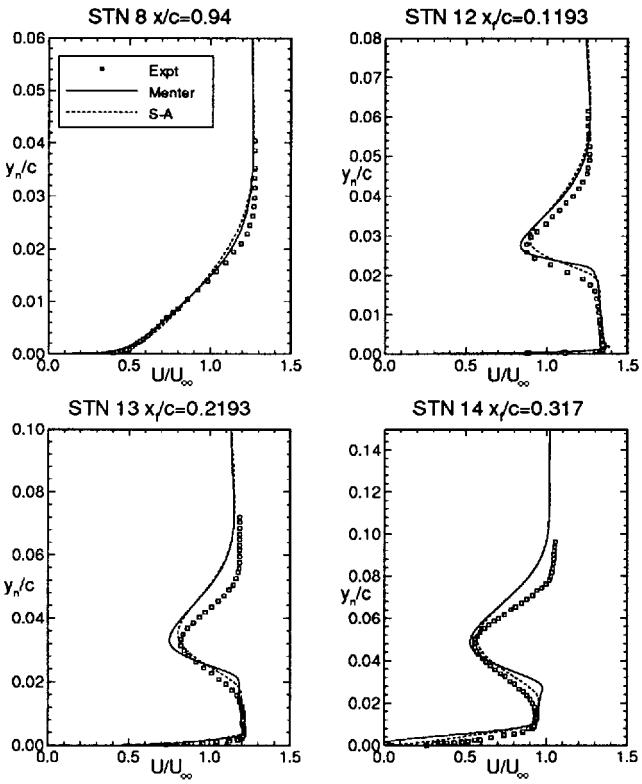

Fig. 14 Boundary-layer and wake velocity profiles for the NLR 7301 airfoil with 20-deg flap, $\alpha = 6.0$ deg, and gap = 2.6% chord.

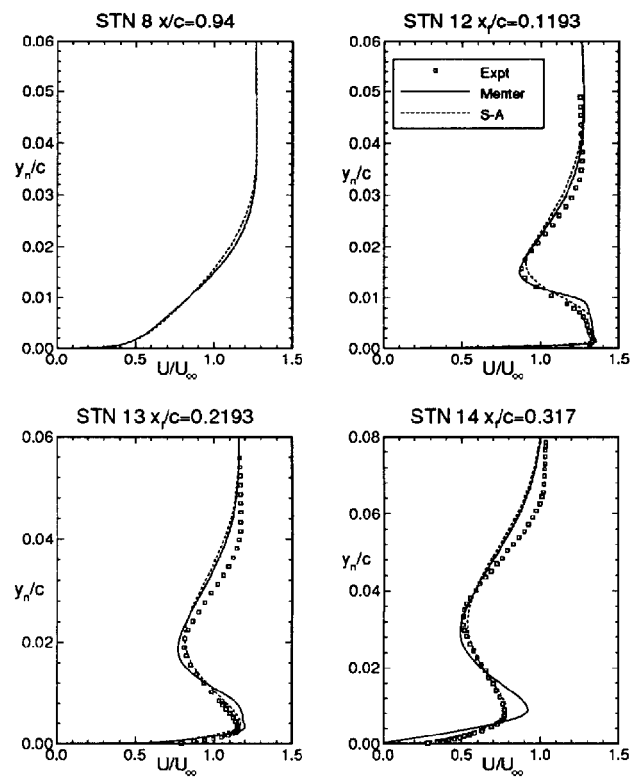

Fig. 15 Boundary-layer and wake velocity profiles for the NLR 7301 airfoil with 20-deg flap, $\alpha = 6.0$ deg, and gap = 1.3% chord.

Boundary-layer and wake profiles at four stations on the upper surface of the airfoil and flap are shown in Fig. 19. The development of the wake of the main airfoil is predicted fairly well by both models. Confluence of the flap boundary layer and the wake of the main section is not important for this case. Most noteworthy is the prediction of the separation bubble on the flap. Although the Menter model predicts a thicker bubble, the difference between the models

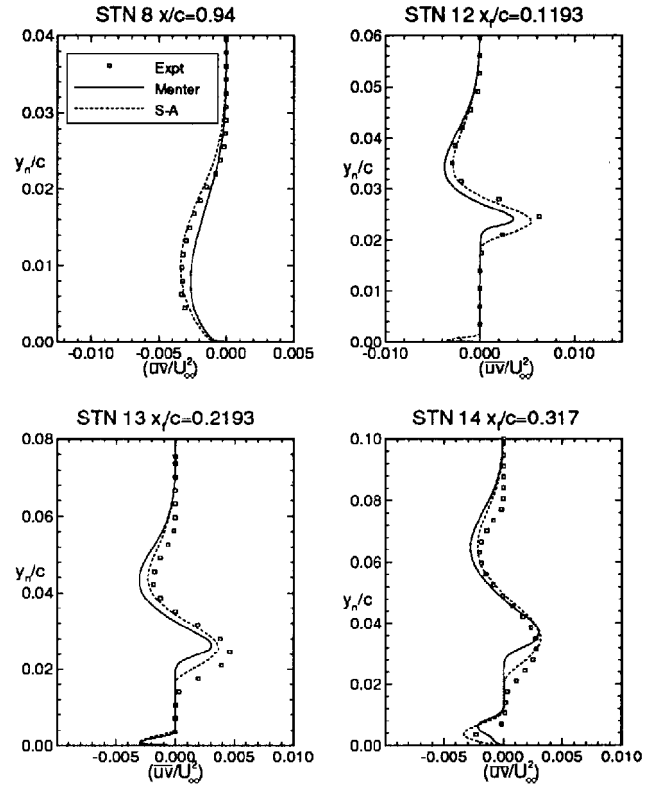

Fig. 16 Turbulent shear stress profiles for the NLR 7301 airfoil with 20-deg flap, $\alpha = 6.0$ deg, and gap = 2.6% chord.

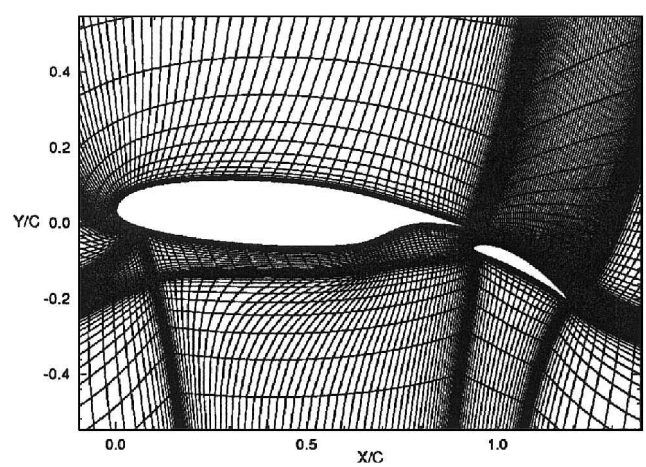

Fig. 17 Near-field grid for the GA(W)-1 airfoil and flap with every second grid line plotted.

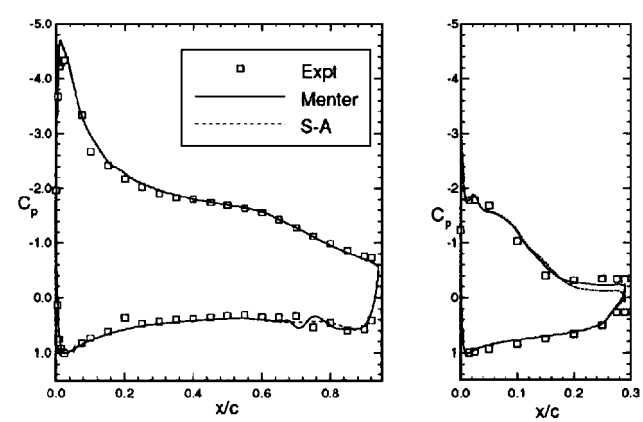

Fig. 18 Pressure distribution on the main airfoil and flap for the GA(W)-1 airfoil with 30-deg flap.

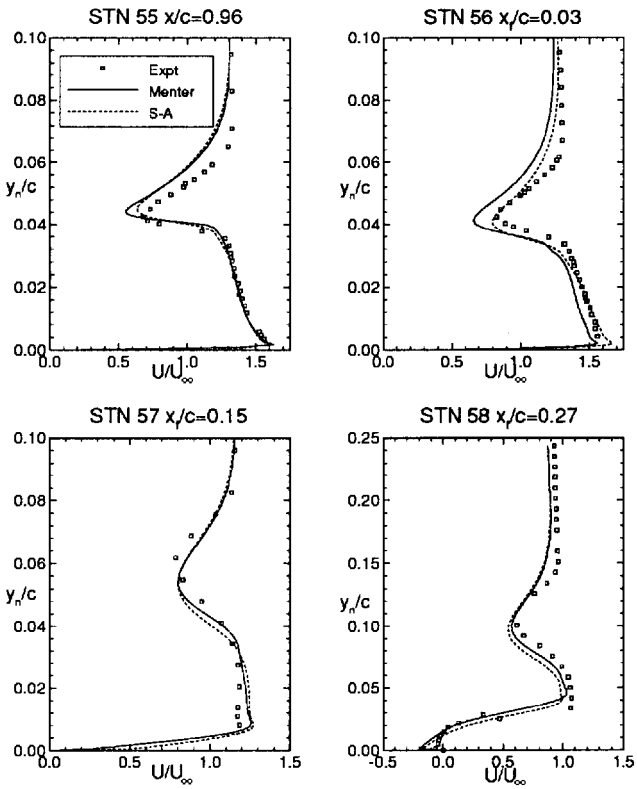

Fig. 19 Boundary-layer and wake velocity profiles for the GA(W)-1 airfoil with 30-deg flap.

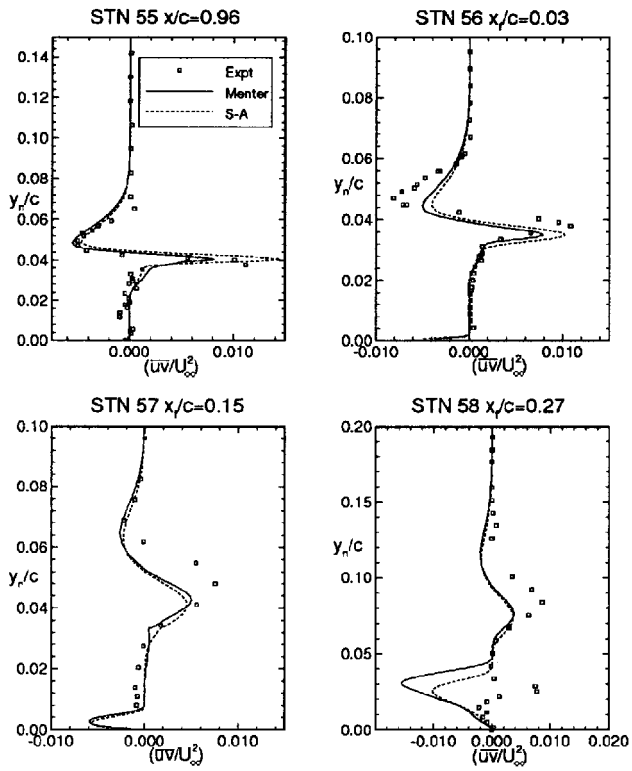

Fig. 20 Turbulent shear stress profiles for the GA(W)-1 airfoil with 30-deg flap.

is not as dramatic as in Fig. 3. Profiles of turbulent shear stress are shown in Fig. 20. Neither turbulence model is particularly accurate in predicting the turbulent shear stress in the wake of the main airfoil.

Conclusions

This paper provides a detailed comparison of the Spalart–Allmaras and Menter turbulence models in the context of two-dimensional high-lift aerodynamic flows. The results show the Menter model to be more accurate in separated flow regions. The Spalart–Allmaras model is more accurate in attached flows and wakes, including merging boundary layers and wakes. The Spalart–Allmaras model is somewhat more robust, though for several cases the computational costs were about equal.

Considering the uncertainties associated with the experimental data and the use of the thin-layer approximation as well as the limitations on the grid resolution that can be used, the performance of these two turbulence models is excellent and represents the state of the art for this application. The Spalart–Allmaras model is preferred for general computations of aerodynamic flows, whereas the Menter model is the better choice if separated flows are of primary interest. Therefore, from a practical standpoint, the Spalart–Allmaras model is appropriate for flap settings typical of takeoff, whereas the Menter model is preferred for analysis of landing flap settings.

Acknowledgments

Funding from de Havilland Inc. and the Natural Sciences and Engineering Research Council of Canada is gratefully acknowledged.

References

[1]Baldwin, B., and Lomax, H., "Thin-Layer Approximation and Algebraic Model for Separated Turbulent Flows," AIAA Paper 78-257, Jan. 1978.

[2]Johnson, D. A., and King, L. S., "A Mathematically Simple Turbulence Closure Model for Attached and Separated Turbulent Boundary Layers," *AIAA Journal*, Vol. 23, No. 11, 1985, pp. 1684–1692.

[3]Baldwin, B. S., and Barth, T. J., "A One-Equation Turbulence Transport Model for High Reynolds Number Wall-Bounded Flows," NASA TM 102847, Aug. 1990.

[4]Spalart, P. R., and Allmaras, S. R., "A One-Equation Turbulence Model for Aerodynamic Flows," AIAA Paper 92-0439, Jan. 1992.

[5]Rogers, S. E., Menter, F. R., Durbin, P. A., and Mansour, N. N., "A Comparison of Turbulence Models in Computing Multi-Element Airfoil Flows," AIAA Paper 94-0291, Jan. 1994.

[6]Holst, T. L., "Viscous Transonic Airfoil Workshop Compendium of Results," AIAA Paper 87-1460, June 1987.

[7]Menter, F. R., "Zonal Two-Equation k-ω Models for Aerodynamic Flows," AIAA Paper 93-2906, July 1993.

[8]Menter, F. R., and Rumsey, C. L., "Assessment of Two-Equation Turbulence Models for Transonic Flows," AIAA Paper 94-2343, July 1994.

[9]Nelson, T. E., Zingg, D. W., and Johnston, G. W., "Compressible Navier–Stokes Computations of Multielement Airfoil Flows Using Multiblock Grids," *AIAA Journal*, Vol. 32, No. 3, 1994, pp. 506–511.

[10]Rentze, K. J., Buning, P. G., and Rajagopalan, R. G., "A Comparative Study of Turbulence Models for Overset Grids," AIAA Paper 92-0437, Jan. 1992.

[11]Anderson, W. K., and Bonhaus, D. L., "Navier–Stokes Computations and Experimental Comparisons for Multielement Airfoil Configurations," AIAA Paper 93-0645, Jan. 1993.

[12]Shima, E., Egami, K., and Amano, K., "Navier–Stokes Computation of a High Lift System Using Spalart–Allmaras Turbulence Model," AIAA Paper 94-0162, Jan. 1994.

[13]Rogers, S. E., Wiltberger, N. L., and Kwak, D., "Efficient Simulation of Incompressible Viscous Flow over Single and Multi-Element Airfoils," AIAA Paper 92-0405, Jan. 1992.

[14]Rogers, S. E., "Progress in High-Lift Aerodynamic Calculations," AIAA Paper 93-0194, Jan. 1993.

[15]Nelson, T. E., Zingg, D. W., and Johnston, G. W., "Navier–Stokes Computations for Multielement Airfoils at Transonic Speeds," *Proceedings of CFD94*, CFD Society of Canada, Toronto, ON, Canada, 1994, pp. A1-01(1)–A1-01(8).

[16]Nelson, T. E., Godin, P., and Zingg, D. W., "Multi-Element Airfoil Computations with One-Equation Turbulence Models," AIAA Paper 95-0357, Jan. 1995.

[17]Valarezo, W. O., and Mavriplis, D. J., "Navier–Stokes Applications to High-Lift Airfoil Analysis," *Journal of Aircraft*, Vol. 32, No. 3, 1995, pp. 618–624.

[18]Doiron, M. D., and Zingg, D. W., "Turbulent Flow Measurements with a Triple-Split Hot-Film Probe," *AIAA Journal*, Vol. 32, No. 9, 1994, pp. 1929–1931.

[19]Van den Berg, B., "Boundary Layer Measurements on a Two-Dimensional Wing with Flap," National Aerospace Lab., NLR TR 79009 U, Amsterdam, The Netherlands, Jan. 1979.

[20]Braden, J. A., Whipkey R. R., Jones, G. S., and Lilley, D. E., "Experimental Study of the Separating Confluent Boundary-Layer," Vol. 1—NASA CR 3655, Vol. 2—NASA CR 166018, March 1983.

[21]Pulliam, T. H., "Efficient Solution Methods for the Navier–Stokes Equations," *Numerical Techniques for Viscous Flow Computation in Turbomachinery Bladings*, Lecture Notes for the Von Kármán Inst. for Fluid Dynamics Lecture Series, Von Kármán Inst. for Fluid Dynamics, Rhône-Saint-Génèse, Belgium, Jan. 1986.